polymer papers

A broad line n.m.r. study of oriented poly(vinylidene fluoride)

J. Clements, G. R. Davies and I. M. Ward
Department of Physics, University of Leeds, Leeds LS2 9JT, UK
(Received 28 March 1984; revised 15 June 1984)

Broadline nuclear magnetic resonance measurements have been carried out for the proton resonance in oriented poly(vinylidene fluoride). The spectra in general show two component lines with distinctly different line widths. The broad component shows a high degree of molecular orientation and can be satisfactorily assigned to the crystalline regions of the polymer. The narrow component corresponds to an oriented non crystalline phase which is sufficiently constrained to allow motion about the chain axis only. An appreciable decrease in the value of the rigid mass fraction was observed in both of the samples over the temperature range examined. Our calculations indicate that this could play an important role in the temperature dependence of the pyroelectric response of this material.

(Keywords: broad line n.m.r.; oriented polyvinylidene fluoride)

INTRODUCTION

There has been exceptional interest in the structural characterization of poly(vinylidene fluoride) (PVDF) because of the potential applications for its piezo-electric and pyroelectric properties[1-5]. Many studies have concentrated on the use of X-ray diffraction to determine the various crystallographic forms which can occur, depending on thermal and mechanical treatment. These forms have also been examined by infra-red and Raman spectroscopy[6,7].

These structural studies have clearly established that the presence of a polar crystal form plays a vital role in the electical response. It is also clear, however, that the origins of this response are complex, and that satisfactory quantitative explanations require an understanding of the contribution from several possible mechanisms. The investigation described in the present paper was initiated to examine one specific aspect, the possible decrease in polarisation with increasing temperature due to changes in molecular mobility. Broad line nuclear magnetic resonance is being used to explore the situation and the present paper describes in detail the determination of the rigid fraction of material as a function of temperature.

Two samples were selected for examination over a range of temperatures. One sample has a very high proportion of Form I and has been drawn at high temperatures to give a high degree of orientation and a high Young's modulus. Such samples have been shown to give, after poling, a high pyroelectric response[8]. The second sample also has a high Form I content but has been drawn at lower temperatures to give almost as high crystalline orientation but lower Young's modulus. Such samples have been shown to possess a rather lower pyroelectric response[8].

The n.m.r. results are also of some interest in their own right, in particular with regard to the determination of molecular orientation and this relates to previous studies on polyethylene and other polymers. They also have some relevance to previous n.m.r. studies from this laboratory and elsewhere which had different objectives to the present work[9-12].

EXPERIMENTAL

For the reasons already discussed, it was desirable to produce highly oriented samples, with a very high Form I content. It has been shown that PVDF films drawn to a draw ratio of 6 at a temperature of 140°C, with a Young's modulus of $\approx$4 GPa, when suitably poled will show a pyroelectric coefficient λ of typically 35 $\mu Cm^{-2}K^{-1}$. As indicated above, samples drawn to a lower draw ratio of 4 at 80°C, show a Young's modulus of $\approx$2.5 GPa, and a significantly lower pyroelectric coefficient, when poled to give the optimum electrical response.

For the n.m.r. measurements two homogeneous cylindrical samples of comparable orientation and structure to those described above were prepared by die-drawing. Isotropic billets of PVDF were prepared by injection moulding at 215°C using a standard commercial grade of polymer (Solvay-Cie, Belgium. Grade Solef X10N; $M_n = 171\,000$, $M_w = 351\,000$). The initial billets were then drawn through a conical die (a) with a die temperature of 140°C and a draw extension of 40 mm min^{-1}, to a draw ratio of 6, and a modulus of $\approx$4 GPa, (b) with a die temperature of 80°C and a draw extension of 10 mm min^{-1}, to a draw ratio of 4, and a modulus of 2.8 GPa. Full details of the die-drawing procedures are described in separate publications[13,14].

N.m.r. measurements

The n.m.r. investigation was carried out using a Varian DP60 spectrometer operated at 60 MHz. A time averaging computer was used to add together the signals from several successive sweeps through the spectrum to improve the signal to noise ratio.

The sample took the form of a short rod 6 mm long and 5 mm in diameter. This was placed in a circular slot machined into a 6 mm diameter PTFE rod, so that the

0032-3861/85/020208-11$03.00

draw direction of the sample was perpendicular to the PTFE rod. The orientation of the specimen with respect to the magnetic field could therefore be varied by rotating the PTFE rod in the n.m.r. spectrometer probe, the angle between the sample draw direction and the static magnetic field being measured by a goniometer head attached to the PTFE rod. The magnetic field sweep was calibrated using the side bands produced by modulating the transmitter frequency at 21.289 kHz and running a spectrum at low modulation, for a sample of glycerine. The modulation produced side bands at 60 MHz $\pm$ n(21.289 kHz) which appear at 5 Gauss intervals in the recorded spectrum. The average field interval at which the signal was recorded was about 0.04 Gauss. The modulation amplitude was calibrated by measuring the separation of the maximum and minimum of the derivative signal of a glycerine sample. The values of second moments were thus corrected for a modulation amplitude of 0.64 Gauss, using the Andrew correction[15].

Recording of n.m.r. spectra above room temperature was achieved using a Varian Variable Temperature Controller. For this purpose, dry nitrogen gas is heated to the selected temperature by a heater in the probe.

Radio frequency power levels were chosen to be well below those producing saturation by making preliminary measurements at different power levels at all temperatures, and checking that symmetrical derivative signals were observed.

Wide angle X-ray diffraction measurements

Wide angle X-ray diffraction (WAXS) measurements were used to obtain a direct measure of the orientation of the crystalline regions. As the samples possess fibre symmetry, this can be done most conveniently by observations on the *001* reflection for Form I PVDF. In this investigation the measurements were carried out with a Siemens Type F wide angle X-ray diffractometer. Appropriate orientation averages $\langle P_2(\cos\Delta)\rangle$ and $\langle P_4(\cos\Delta)\rangle$ were evaluated from such measurements.

The concentration of Form I crystals was also obtained by X-ray diffraction, using the method devised by Davies and Singh[16].

THEORY

Calculation of the rigid lattice second moment for oriented Form I PVDF

The second moment of the n.m.r. absorption may be calculated from purely theoretical considerations, using the analysis due to Van Vleck[17]. This calculation requires a knowledge of the spatial coordinates of the resonating nuclei together with certain fundamental constants. The Van Vleck second moment formula for the resonance of one type of magnetic species on a crystal lattice containing two types of magnetic species can be written

$$\langle \Delta H^2\rangle = \frac{6}{5} I(I+1) g^2 \mu_n^2 N^{-1} \sum_{j>k} r_{jk}^{-6} (3\cos^2\beta_{jk} - 1)^2 + \frac{4}{15} I_f(I_f+1) g_f^2 \mu_n^2 N^{-1} \sum_{j,f} r_{jf}^{-6} (3\cos^2\beta_{jf} - 1)^2$$

where I and I_f are nuclear spin numbers, g and g_f nuclear g-factors, μ_n is the nuclear magneton, N the number of magnetic nuclei over which the sum is taken, r_{jk} and r_{jf} the lengths of the vectors joining nucleus j with nuclei k and f respectively and β_{jk} and β_{jf} the angles between vectors r_{jk} and r_{jf} and the direction of the externally applied magnetic field H. It should be noticed that the numerical coefficient for the contribution to the second moment from pairs of identical nuclei is 9/2 times greater than for unlike pairs. One expects a trivial difference of a factor 2 in these coefficients since the sum is arranged to count each pair of nuclei once only. The real difference is therefore a factor 9/4, which is the square of the factor 3/2 arising from the mutual spin exchange process which can only take place between identical nuclei.

If we wish to examine the anisotropy of the second moment about the direction of the magnetic field we must express the Van Vleck equation in terms of (a) the orientation distribution functions which describe the orientation of the crystallites within the material, (b) the orientation of the material as a whole with respect to the static magnetic field. Here we will draw upon the analysis performed by McBrierty and Ward[10], presenting only their final results. Imagine that the partially oriented polymer consists of an aggregate of units of structure. Uniaxial drawing produces an oriented structure which a variety of physical measurements show to possess transverse isotropy, and there is no preferential orientation of the units of structure in a plane perpendicular to the draw direction. The Van Vleck formula for the second moment now becomes

$$\langle \Delta H^2\rangle = \sum_{l=0,2,4} \frac{4\pi a_l}{2l+1} \mu_n^2 Y_{l0}(\gamma) \langle P_l(\cos\Delta)\rangle \times [I_1(I_1+1) g_1^2 S_{l0}^{11} + (4/9) I_2(I_2+1) g_2^2 S_{l0}^{12}]$$

where S_{l0}^{11} and S_{l0}^{12} are the lth lattice sums for interactions between like (S^{11}) and unlike (S^{12}) nuclei

$$S_{l0} = \sum r_{jk}^{-6} Y_{l0}(\theta_{jk})/N$$

the $\langle P_{l0}(\cos\Delta)\rangle$ are average orientation distribution functions and the a_l are constants given by

$$a_0 = 1/5,\ a_2 = 2/7 \text{ and } a_4 = 18/35$$

Y_{l0} are real spherical harmonics given by

$$Y_{l0}(\theta) = \left(\frac{2l+1}{4\pi}\right)^{1/2} P_{l0}(\cos\theta)$$

and P_{l0} are Legendre polynomials, hence

$$P_0(\cos\theta) = 1,\ P_2(\cos\theta) = \tfrac{1}{2}(3\cos^2\theta - 1)$$
$$P_4(\cos\theta) = \tfrac{1}{8}(35\cos^4\theta - 30\cos^2\theta + 1)$$

The lattice sums $S_{l0}{}^{11}$ and $S_{l0}{}^{12}$ can be calculated from a knowledge of the spatial coordinates of the resonating nuclei. We have done this utilising a computer programme devised and written by Mr I. S. Davidson. It is written in Algol 68 and the calculations were performed on the Amdahl computer of the University of Leeds Computing Service. The program requires as input the nuclear coordinates of the resonant nuclei in a unit cell along with the unit cell parameters. We have used the information provided by Hasegawa *et al.*[8] for Form I

Table 1 Structural information used in the lattice sum calculation

Proton coordinates		
x/a	*y/b*	*z/c*
+0.105	−0.124	0.000
−0.105	−0.124	0.000
+0.605	+0.376	0.000
+0.395	+0.376	0.000
Fluorine coordinates		
x/a	*y/b*	*z/c*
+0.126	+0.355	+0.500
−0.126	+0.355	+0.500
+0.626	+0.855	+0.500
+0.374	+0.855	+0.500
Unit cell dimensions		
a = 8.45 Å	b = 4.91 Å	c = 2.56 Å
$\alpha = 90°$	$\beta = 90°$	$\gamma = 90°$

Table 2 Calculated lattice sums

S_{00}^{11}	0.0059	S_{00}^{12}	0.0028
S_{20}^{11}	−0.0022	S_{20}^{12}	−0.0009
S_{40}^{11}	0.0076	S_{40}^{12}	0.0016

PVDF which is summarized in *Table 1*. The lattice sums have been calculated for all interactions inside a sphere of radius 10 Å and are shown in *Table 2*. Apart from different normalizing factors these numbers are identical to those in Table II of the paper by Douglas, McBrierty and Wang[19].

Calculation of crystallinity

The following procedure was developed for the decomposition of the composite n.m.r. signal into two components, a broad component associated with the rigid crystalline regions and a narrow component associated with mobile non-crystalline material. It was assumed that the crystalline regions give rise to an n.m.r. signal which can be considered to be a Pake doublet, associated with the proton pairs in the $-CH_2-CF_2-$ sequence, this doublet being broadened by the intermolecular interactions and other intramolecular interactions to give a 'Gaussian' doublet line shape as proposed by Manuel and Pranadi for isotropic polyethylene[20]. Following the method of Manuel and Pranadi the Gaussian doublet line shape may be defined as follows:

$$Y(\Delta H)=a_1\left[\exp\left[\frac{(\Delta H-a_2)^2}{2a_3^2}\right]+\exp\left[\frac{(\Delta H+a_2)^2}{2a_3^2}\right]\right]$$

It consists of the superposition of two identical Gaussian line shapes whose centres are separated by a field interval $2a_2$ and whose individual second moments about their centres are a_3^2. The area under this composite curve is $(8\pi)^{1/2}a_1a_3$ and the second moment is $\langle\Delta H^2\rangle = a_2^2+a_3^2$. The variable $\Delta H = H - H_0$ where H_0 is the magnetic field at the centre of the doublet. This line shape was fitted to the outer part of the experimental line with a_1, a_2 and a_3 as adjustable parameters, using a least squares procedure with parabolic extrapolation described by Bevington[21] by minimizing the sum

$$\chi^2=\sum_i\frac{[A_i-Y(\Delta H_i)]^2}{\sigma_i^2}$$

where A_i is the experimental value of the absorption line at the ith point and $Y(\Delta H_i)$ the corresponding value of the Gaussian doublet. χ^2 can be considered as a function of a_1, a_2 and a_3 represented by a 3-dimensional hypersurface which must be searched for a minimum. One of the difficulties is that there may be several local minima for χ^2 among which we require the global minimum. The search for this global minimum involves choosing initial values for the parameters a_1, a_2 and a_3. However, the minimum found depends upon this initial choice, so it becomes necessary to vary the initial values used to find the global minimum of χ^2. The initial values of a_2 and a_3 were chosen by calculating the value of a_2 appropriate to a pair of protons in a CH_2 groups and then deriving a_3 from the theoretical second moment for perfectly oriented Form I PVDF using $\Delta H^2 = a_2^2 + a_3^2$. With these parameters chosen, the choice of an initial value for a_1 could easily be made. A range of initial values of the a_n was used to establish the best overall fit using different ranges of the outer part of the absorption line. Gaussian doublets fitted in the range 5–14 Gauss were found to be the optima. Confirmation of the satisfactory nature of this fitting procedure was more difficult to establish in the present work, than it was for Manuel and Pranadi. They were able to examine the ratios of the squares of the second moment to the fourth moment for the Gaussian doublet fitted, and compare those values with values obtained from theoretical considerations. Since calculation of fourth moments

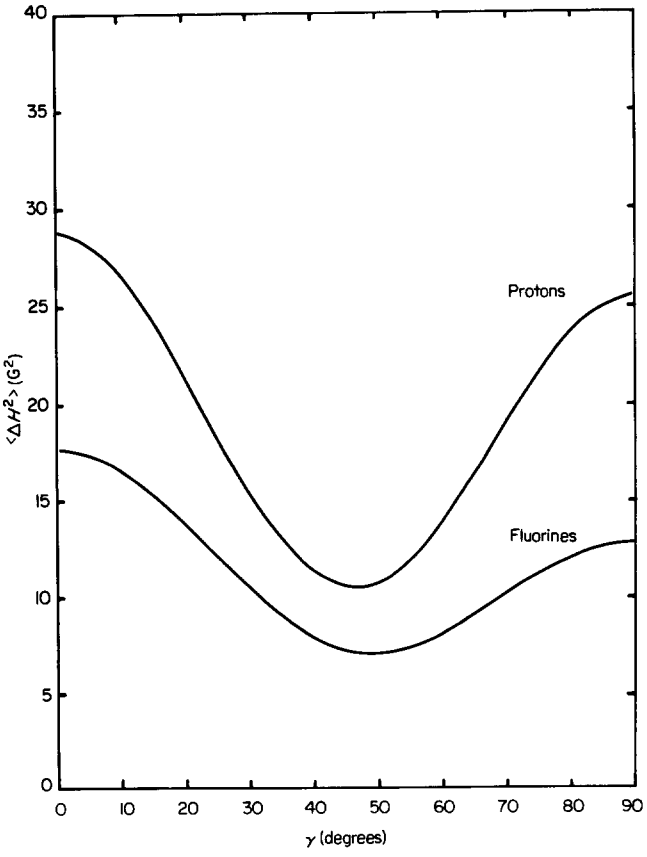

Figure 1 Variation of second moments $\langle\Delta H^2\rangle_c$ for crystalline poly(vinylidene fluoride) with full c axis orientation along the draw direction and transverse isotropy

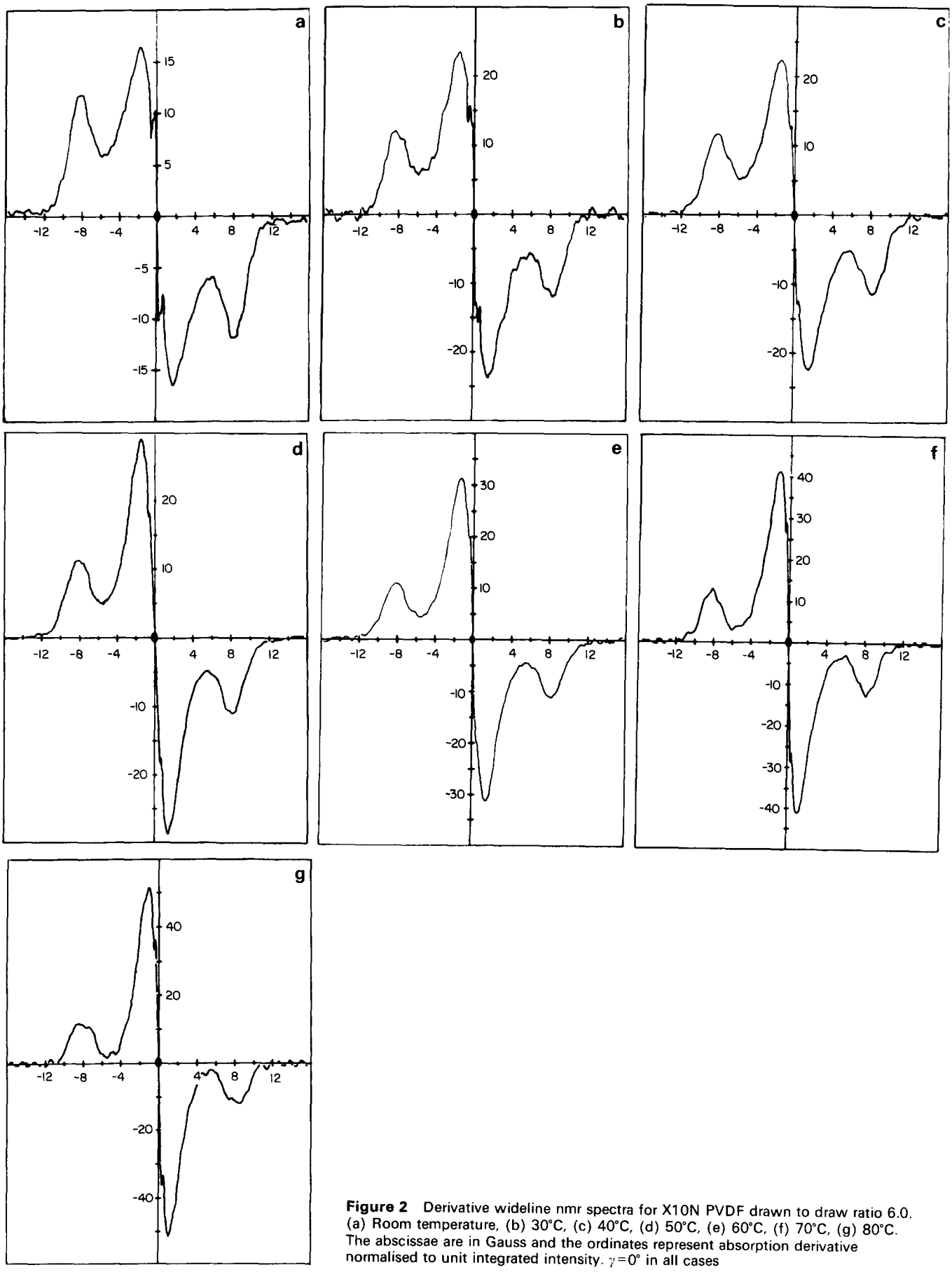

Figure 2 Derivative wideline nmr spectra for X10N PVDF drawn to draw ratio 6.0. (a) Room temperature, (b) 30°C, (c) 40°C, (d) 50°C, (e) 60°C, (f) 70°C, (g) 80°C. The abscissae are in Gauss and the ordinates represent absorption derivative normalised to unit integrated intensity. $\gamma = 0°$ in all cases

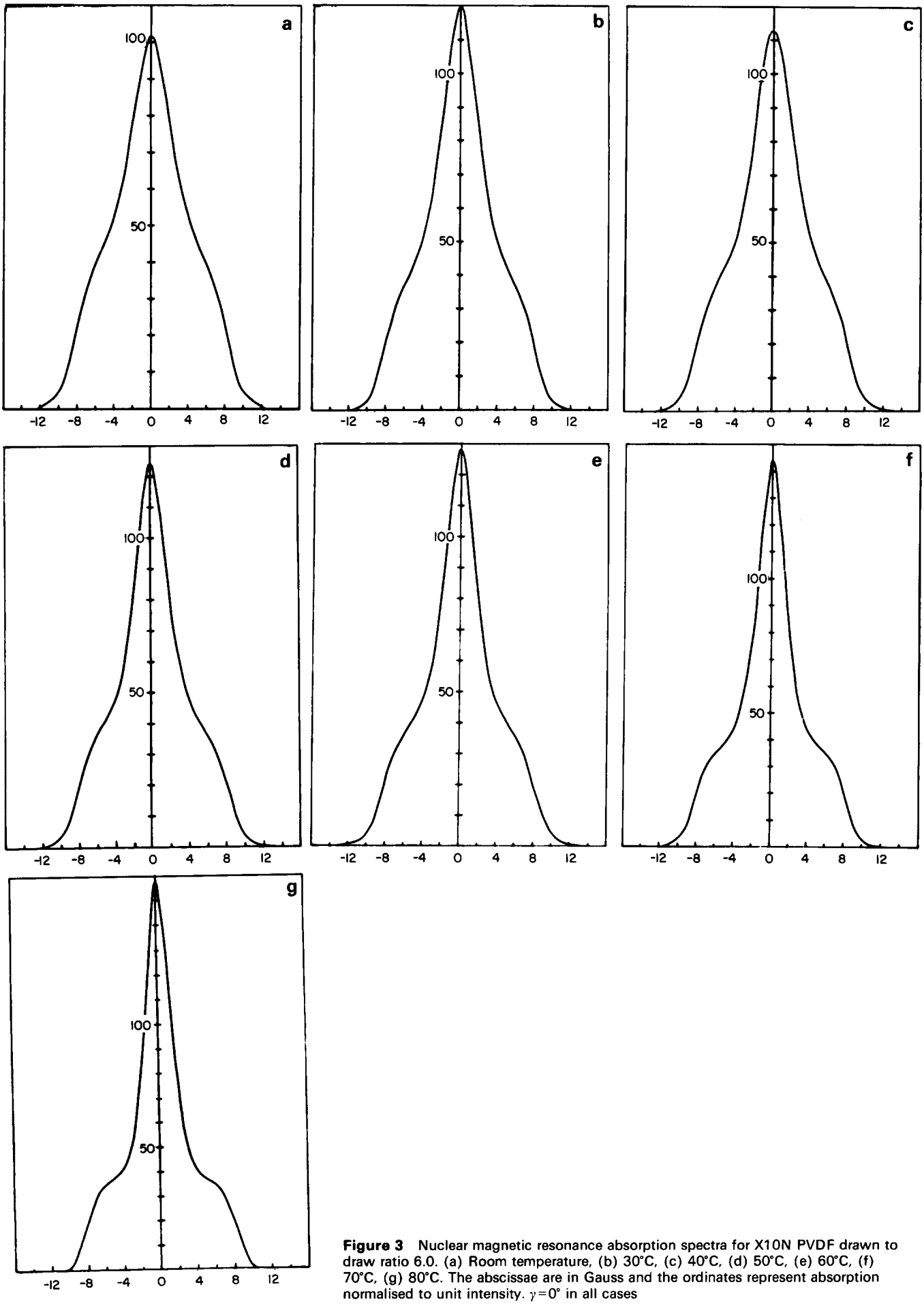

Figure 3 Nuclear magnetic resonance absorption spectra for X10N PVDF drawn to draw ratio 6.0. (a) Room temperature, (b) 30°C, (c) 40°C, (d) 50°C, (e) 60°C, (f) 70°C, (g) 80°C. The abscissae are in Gauss and the ordinates represent absorption normalised to unit intensity. $\gamma = 0°$ in all cases

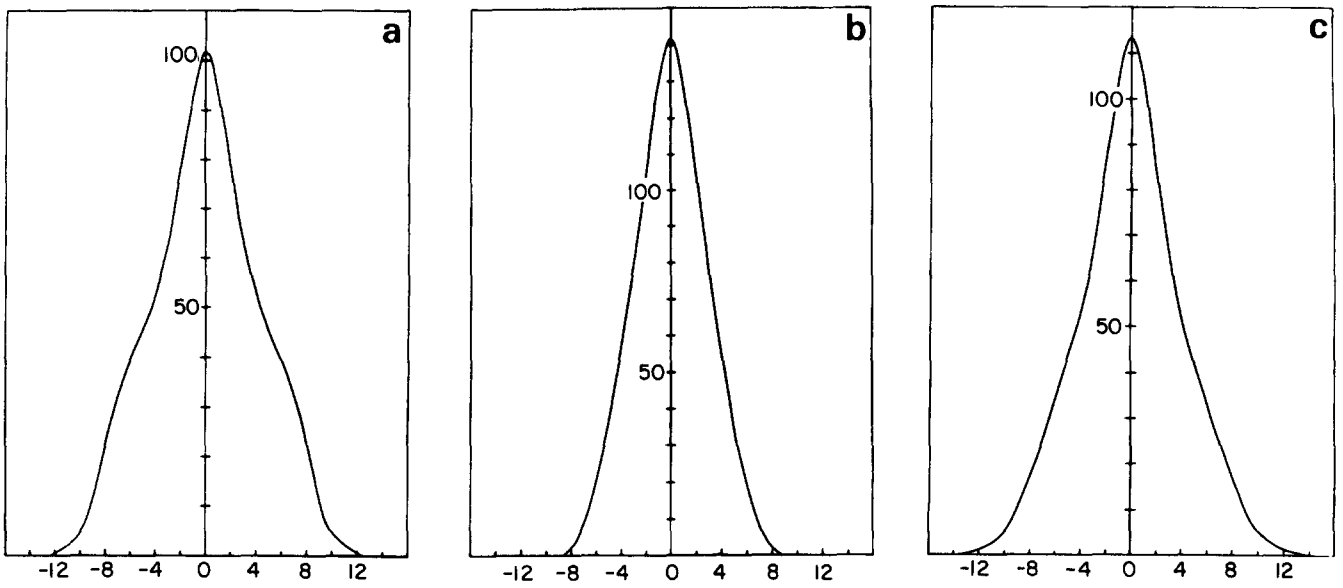

Figure 4 Nuclear magnetic resonance absorption spectra for X10N PVDF drawn to draw ratio 6 for three orientations with respect to the magnetic field $\gamma = 0$, 45 and 90°. Room temperature spectra. (a) $\gamma = 0°$, (b) $\gamma = 45°$, (c) $\gamma = 90°$. The abscissae are in Gauss and the ordinates represent absorption normalised to unit integrated intensity

for oriented systems is a very arduous task indeed it was decided to examine the variation of second moment with the angle between the sample draw direction and the static magnetic field and (a) compare this with the theoretical variation derived for a perfectly oriented system, (b) calculate values of $\langle P_2(\cos\Delta)\rangle$ and $\langle P_4(\cos\Delta)\rangle$ (or $\langle\cos^2\Delta\rangle$ and $\langle\cos^4\Delta\rangle$) and compare these with values obtained from X-ray diffraction measurements.

For a perfectly uniaxially oriented sample of PVDF we can calculate the anisotropy of the second moment with respect to the magnetic field, because $\langle P_l(\cos\Delta)\rangle$ in the Van Vleck formula are equal to unity for all l. We have done this and the results are shown in *Figure 1* as a function of γ. We have included both proton resonance and fluorine resonance for interest.

From experimental determinations of second moment anisotropy, and knowing values of the lattice sums we are able to estimate values of $\langle P_l(\cos\Delta)\rangle$ for the rigid component and hence $(\cos^2\Delta)$ and $(\cos^4\Delta)$ for direct comparison with values obtained from X-ray diffraction measurements. It is in this way that we are able to establish the reliability of our Gaussian doublet fitting procedures and hence our measurements of crystallinity.

RESULTS AND DISCUSSION

General nature of the n.m.r. results

Figures 2(a)–2(g) show the derivative spectra and *Figures 3(a)–3(g)* the corresponding absorption spectra for the sample draw direction aligned parallel to the static magnetic field ($\gamma = 0$ degrees direction) for the higher draw ratio sample. Results are presented for all temperatures of measurement between room temperature and +80°C. The spectra may be compared directly since they have all been normalized to give unit (integrated) intensity. It is clear that all spectra are composite and the simplest interpretation is that a broader doublet is superimposed on a narrower singlet. The intensity of the broader doublet is clearly reduced relative to the narrow component as the temperature is increased.

The existence of two distinct components of differing widths is consistent with a rigid lattice component and a mobile component. The broad component is readily identified as a doublet associated with the crystalline regions and we shall show that the second moments of the spectra are consistent with this interpretation. The narrower line is less easily defined. As will be discussed later it shows some angular dependence, and therefore must be associated with a partially oriented mobile phase.

Figures 4a–c, and *Figures 5a–c* show the absorption spectra for the draw direction at $\gamma = 0$, 45 and 90° to the static magnetic field, at room temperature and at +80°C, again for the higher draw ratio samples. The two components of the spectra are noticably better resolved in the $\gamma = 0$ spectra at both temperatures and for this reason we adopted the following approach. First, the two components were separated at $\gamma = 0$ to give values of the mass fractions of both components. These decompositions were then used as a guide to facilitate the decompositions at other orientations, though we only attempted these decompositions at room temperature before heating the sample, at +80°C, and at room temperature after heating the sample. The total measured second moment was then divided into contributions from the rigid (or crystalline) and mobile components. Decomposition of the spectra at various angles γ, enabled orientation functions for the rigid component to be obtained which in turn were used as a check on that same decomposition procedure.

Determination of the rigid and mobile mass fractions

The proportions of rigid and mobile material at each temperature were determined from the spectra for both samples. The rigid mass fraction f_R is given by the ratio of the integrated intensity of the rigid fraction component (the fitted Gaussian doublet) to the total integrated intensity. The mass fraction of the mobile component is, in this case, the complement of the rigid mass fraction. The spectra at each temperature were decomposed as accurately as possible, those at $\gamma = 0$ being used as a guide where other decompositions were attempted, since the doublet structure is partially resolved because for all the CH_2 groups (which contribute most strongly to the

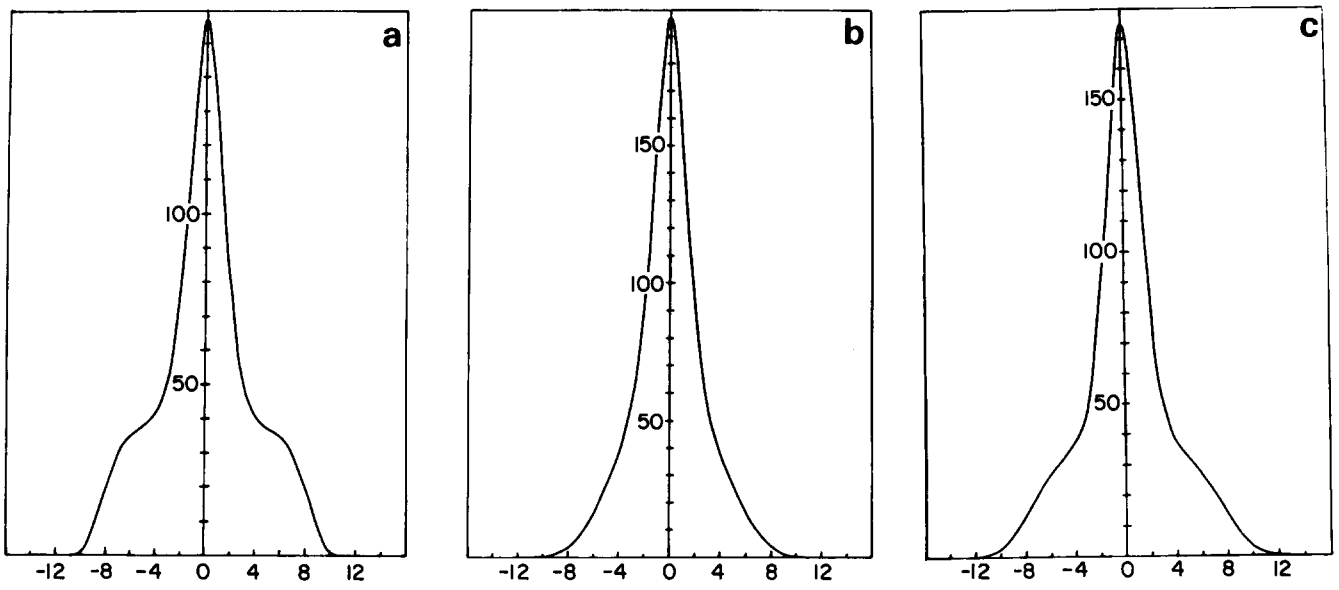

Figure 5 Nuclear magnetic resonance absorption spectra for X10N PVDF drawn to draw ratio 6 for three orientations with respect to the magnetic field $\gamma=0$, 45 and 90°+80°C spectra. (a) $\gamma=0$, (b) $\gamma=45°$, (c) $\gamma=90°$. The abscissae are in Gauss and the ordinates represent absorption normalised to unit integrated intensity

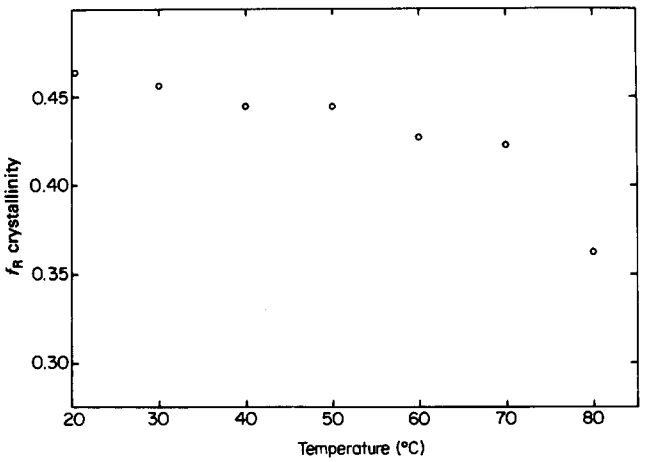

Figure 6 The variation of the rigid mass fraction (crystallinity) f_R as a function of measurement temperature for X10N PVDF $R_A=6.0$

absorption spectra) the internuclear vector joining a pair of protons is closely perpendicular to the direction of the static magnetic field. The variation of the rigid mass fraction (or crystallinity) is shown as a function of measurement temperature in *Figure 6*. We see that the rigid mass fraction decreases with increasing temperature, but that the decrease is not linear. At temperatures above 60°C there is a rapid decrease. Moreover the changes in crystallinity are quite reversible; except for an initial fall in the room temperature value which occurs the first time the sample is heated.

The results of the Gaussian doublet fitting procedure for the higher draw ratio sample together with the numerical values for the rigid fraction f_R are tabulated in *Table 3*. It is of particular interest that the Gaussian breadth parameter a_3 is very nearly constant, independent of the direction of the steady magnetic field, confirming that the inter- and intramolecular interaction are almost constant. Moreover, both a_2 and a_3 are very nearly temperature independent. These results, taken together, afford considerable support for modelling the rigid lattice line shape in this way.

The validity of the decomposition procedure is confirmed by the closeness of the values obtained for the rigid fraction f_R for $\gamma=0$, 45° and 90°, although this procedure is necessarily somewhat arbitrary for $\gamma=45°$ where the resolution of the two components is worst.

Similar results were obtained for the lower draw ratio sample and these are summarised in *Table 4*.

Evaluation of second moment anisotropy and comparison of orientation averages obtained from n.m.r. and X-ray diffraction measurements

The variation with γ of the second moments of the rigid components of the n.m.r. signals were evaluated from the decomposition of spectra recorded at room temperature before heating, at 80°C and at room temperature after cooling. The results obtained at room temperature and 80°C are shown in *Figures 7a–c* and *8* for the high draw ratio and low draw ratio samples respectively.

As mentioned above, it is possible to estimate values of $\langle P_l(\cos\Delta)\rangle$; the orientation distribution functions for the rigid fraction and hence $\langle P_2(\cos\Delta)\rangle$ and $\langle P_4(\cos\Delta)\rangle$ from n.m.r. measurements. It is also possible to estimate these functions from X-ray diffraction measurements directly, which affords us a comparison. The results of this comparison are shown in *Table 5*. A comparison is only possible at room temperature before heating, since X-ray measurement at 80°C was not possible. However, we see that the agreement between the two estimates of $\langle P_2(\cos\Delta)\rangle$ and $\langle P_4(\cos\Delta)\rangle$ is extremely good for both samples.

This measure of agreement between the two methods provides further confidence in the decompositions not only where comparison has been made at room temperature and 80°C, but at the intermediate temperatures. It suggests that the rigid fraction can probably be identified with the crystalline regions.

It is clear from this comparison that there is little or no significant change in $\langle P_2(\cos\Delta)\rangle$ and $\langle P_4(\cos\Delta)\rangle$ as a

Table 3 Fitting parameters for Gaussian doublet and rigid fraction values f_R (High draw ratio sample)

	γ	a_1	a_2	a_3	$\langle\Delta H^2\rangle$	f_R
Room temperature before heating						
	0	0.032	3.61	3.14	22.91	0.503
	45	0.031	1.71	3.23	13.36	0.502
	90	0.031	3.51	3.23	22.81	0.502
30°C	0	0.029	3.66	3.13	23.24	0.458
40°C	0	0.027	3.53	3.27	23.18	0.445
50°C	0	0.024	3.10	3.68	23.19	0.445
60°C	0	0.026	3.61	3.16	23.07	0.427
70°C	0	0.026	3.56	3.27	23.42	0.424
80°C	0	0.024	3.81	3.02	23.62	0.365
	45	0.021	1.72	3.23	13.39	0.342
	90	0.023	3.64	3.14	23.15	0.362
Room temperature after heating						
	0	0.029	3.61	3.14	22.88	0.465
	45	0.029	1.88	3.23	13.97	0.462
	90	0.030	3.60	3.14	22.82	0.468

Each value quoted above is the mean of eight measurements. The standard error in the mean values for a_1, a_2 and a_3 are ±2%. The estimated standard errors in the values of $\langle\Delta H^2\rangle$ and f_R are ± 6%.

Table 4 Fitting parameters for Gaussian doublet and rigid fraction values f_R (Low draw ratio sample)

	γ	a_1	a_2	a_3	$\langle\Delta H^2\rangle$	f_R
Room temperature						
	0	0.036	3.42	2.53	18.12	0.456
	45	0.029	2.49	3.07	15.68	0.452
	90	0.031	3.41	2.96	20.40	0.461
60°C	0	0.0296	3.26	2.85	18.78	0.423
80°C	0	0.0285	3.28	2.83	18.82	0.405

Each value quoted above is the mean of eight measurements. The standard errors in the mean values for a_1, a_2 and a_3 are ±2%. The estimated standard errors in the values of $\langle\Delta H^2\rangle$ and f_R are ± 6%

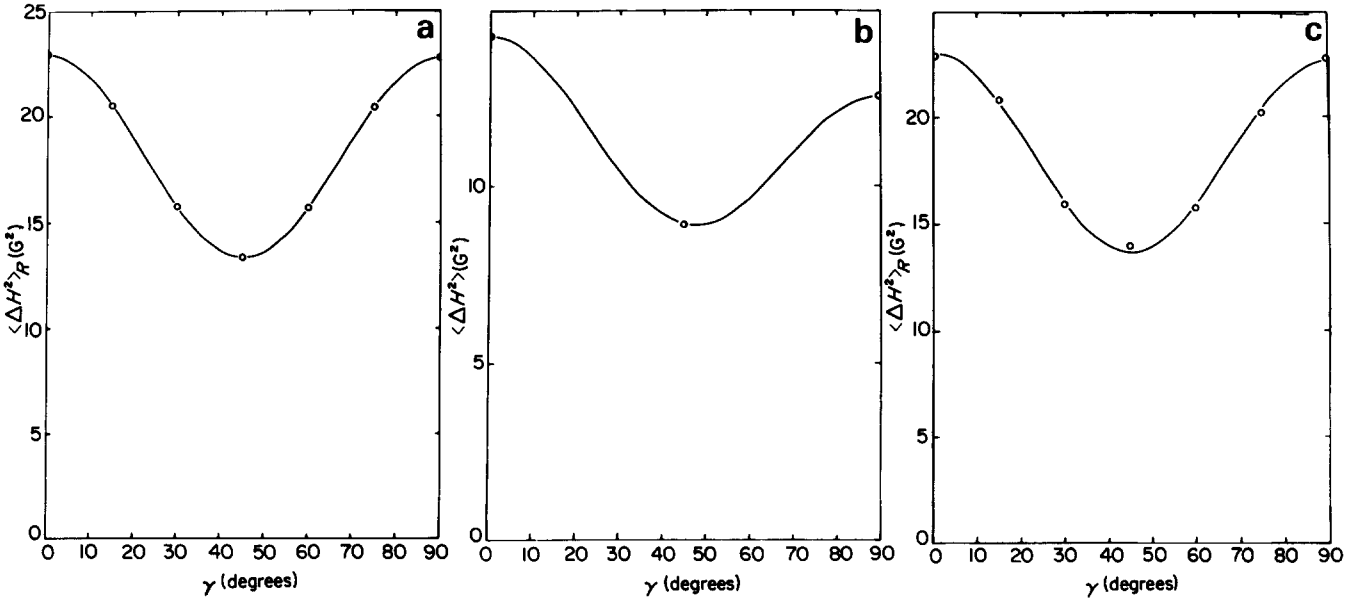

Figure 7 Second moments $\langle\Delta H^2\rangle_R$ of the rigid component as a function of orientation angle γ, deduced as described in the text, for X10N PVDF R_A=6.0. (a) At room temperature before heating; (b) At 80°C; (c) At room temperature after heating

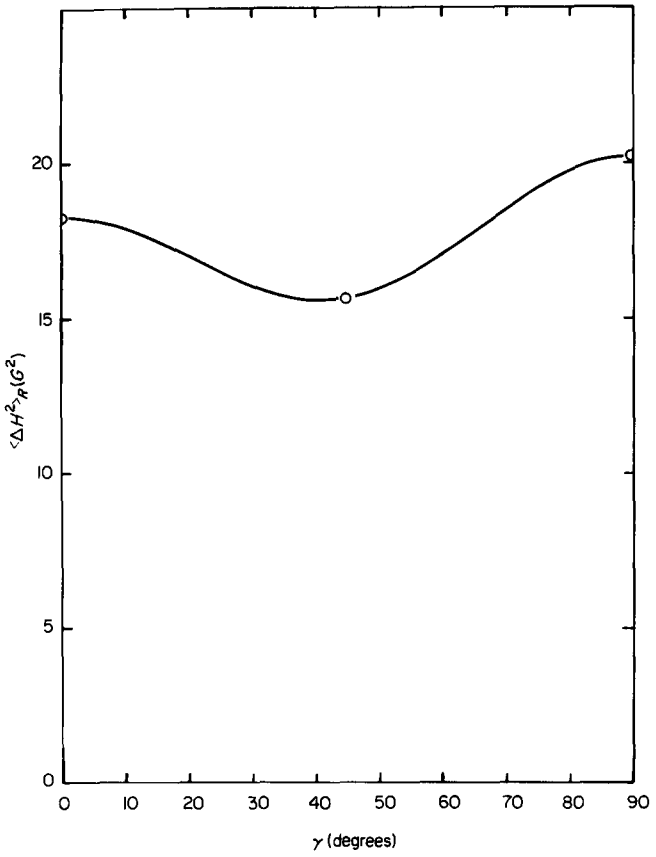

Figure 8 Second moments $\langle\Delta H^2\rangle_R$ of the rigid component as a function of orientation angle γ, deduced as described in the text, for X10N PVDF R_A=4.0. At room temperature before heating

function of temperature. The rigid fraction of this material is reduced by an increase in temperature but the integrity of this component is otherwise maintained.

The mobile component

The second moment of the mobile component $\langle\Delta H^2\rangle_m$ can be obtained from the total second moment $\langle\Delta H^2\rangle$ and the second moment of the rigid component $\langle\Delta H^2\rangle_R$.

$$f_m\langle\Delta H^2\rangle_m=\langle\Delta H^2\rangle-f_R\langle\Delta H^2\rangle_R$$

The variation with γ of the total second moments evaluated before, during and after heating are shown in *Figures 9a–c* and *Figure 10* for the two samples and the corresponding $\langle\Delta H^2\rangle_m$ for the mobile components deduced from them are shown in *Figures 11a–c* and *Figure 12.*

The shapes of the curves of *Figures 11* and *12* show a qualitative similarity with the theoretical calculations of Folkes and Ward for the second moment variation of an assembly of oriented chains undergoing a rotation about their axis[22]. However, the anisotropy of $\langle\Delta H\rangle_m$ is noticeably decreased at high temperatures suggesting that the mobile component is becoming increasingly mobile and more isotropic, more akin to a true amorphous phase.

There is also a very significant difference between the mobility of the mobile fraction in the high and low draw ratio samples. Comparison of *Figures 11(a)* and *12* shows that the mobility in the high draw ratio sample is much reduced. This result is consistent with the higher modulus of this sample and will be discussed quantitatively in a future publication.

Table 5 Orientation function estimated from n.m.r. and X-ray diffraction measurements

Sample	Temperature	$\langle P_2(\cos\Delta)\rangle$ X-ray	n.m.r.	$\langle P_4(\cos\Delta)\rangle$ X-ray	n.m.r.
High draw ratio	Room (before heating)	0.857	0.857	0.847	0.572
	80°C		0.844		0.602
	Room (after heating)		0.712		0.547
Low draw ratio	Room	0.701	0.696	0.215	0.215

The standard error in the n.m.r. estimates of $\langle P_2(\cos\Delta)\rangle$ and $\langle P_4(\cos\Delta)\rangle$ are ±6%. The standard error in the X-ray estimates are ±5%

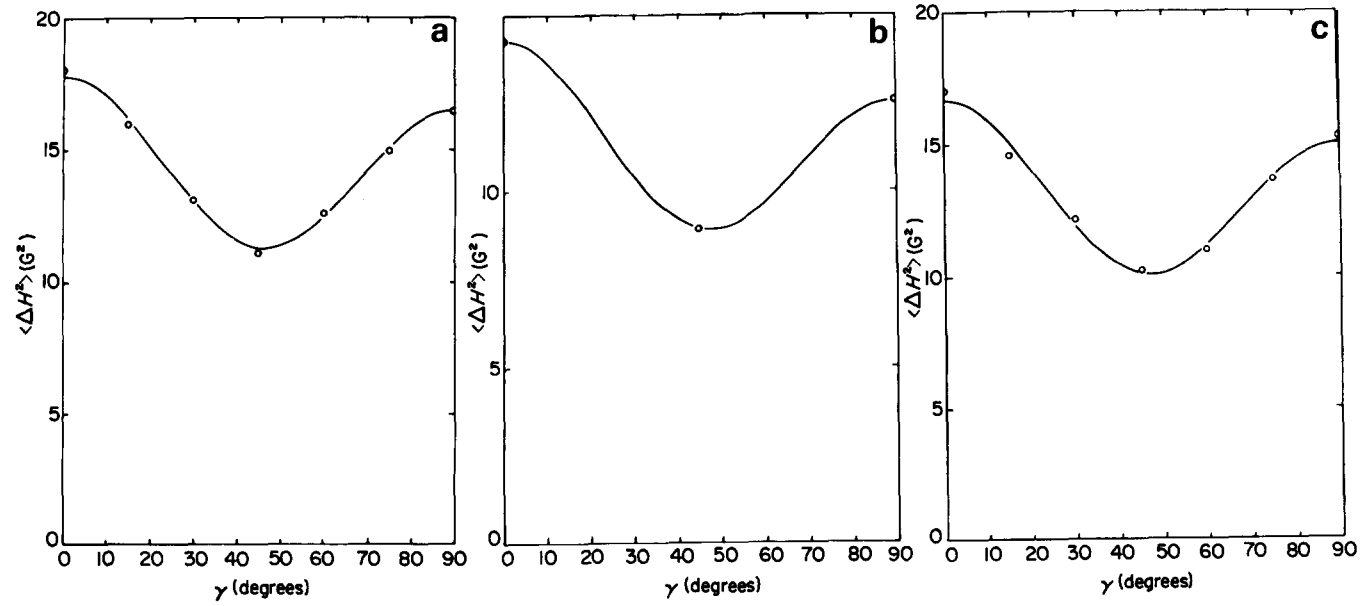

Figure 9 Total second moment $\langle\Delta H^2\rangle$ as a function of orientation angle γ, for X10N PVDF R_A=6.0. (a) At room temperature before heating; (b) At 80°C, (c) At room temperature after heating

Change in rigid fraction with temperature and the possible contributions to the pyroelectric coefficient

The change in rigid fraction f_R for the higher draw ratio sample is from 0.503–0.427 over the temperature range 20–60°C. It falls more rapidly with temperature between 60 and 80°C to a value of 0.365. These results enable us to make an estimate of the maximum effect which the change in rigid fraction with temperature could have on the polarisation per unit volume and hence provide a maximum value for the calibration to the pyroelectric coefficient from this source alone.

An estimate of the polarisation per unit volume for the Form I crystal has been given[4] as 0.25 cm^{-2}. Assuming

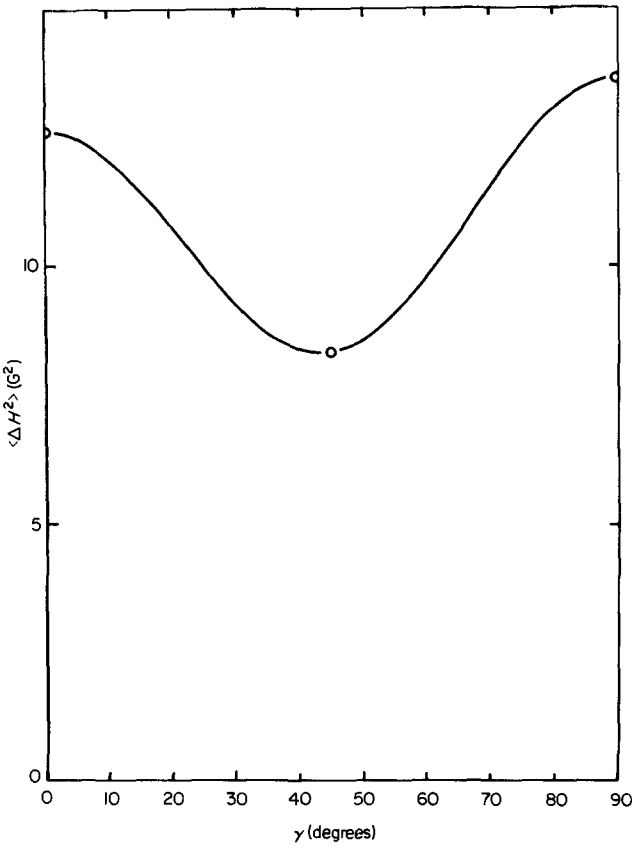

Figure 10 Total second moment $\langle \Delta H^2 \rangle$ as as a function of orientation angle γ, for X10N PVDF R_A=4.0. At room temperature before heating

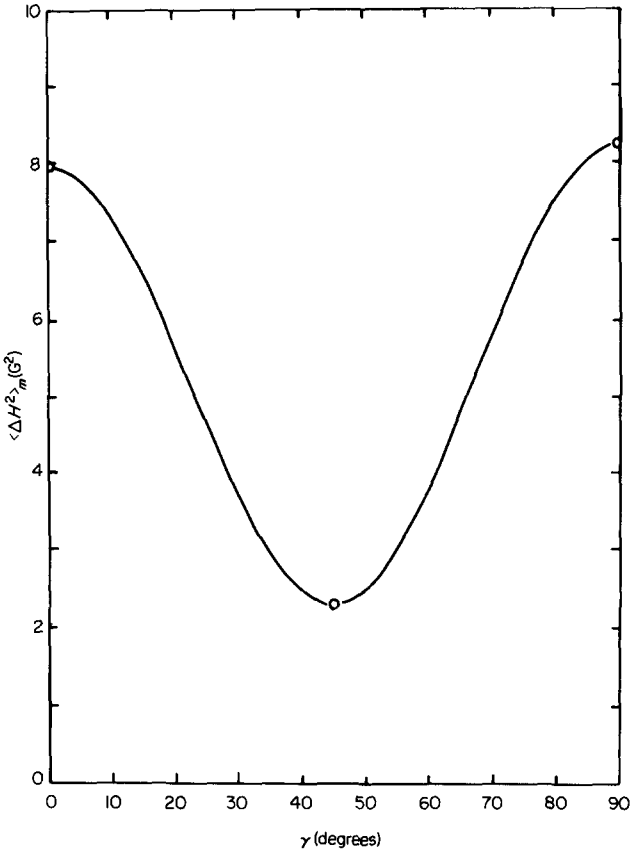

Figure 12 Second moments $\langle \Delta H^2 \rangle_m$ of the mobile component as a function of orientation angle γ, deduced as described in the text, for X10N PVDF R_A=4.0. At room temperature before heating

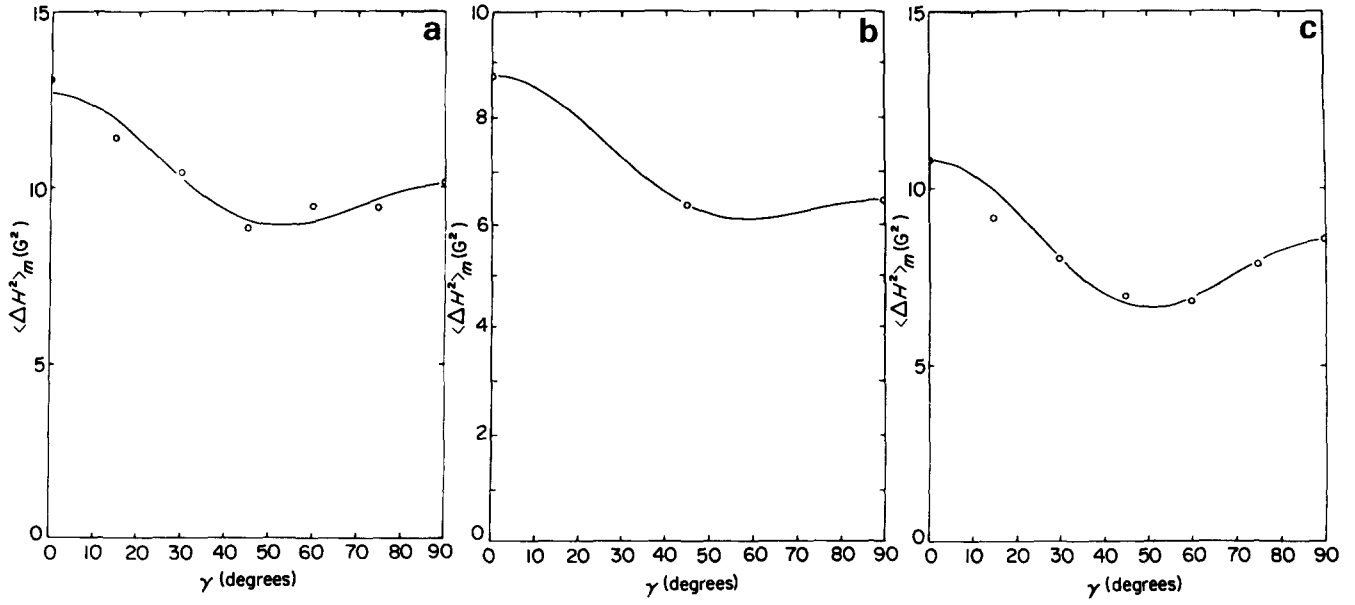

Figure 11 Second moments $\langle \Delta H^2 \rangle_m$ of the mobile component as a function of orientation angle γ, deduced as described in the text, for X10N PVDF R_A=6.0. (a) At room temperature before heating; (b) At 80°C; (c) At room temperature after heating

that the rigid fraction f_R is 0.503 this gives the polarisation per unit volume for an ideal polarised sample as 0.126 cm^{-2}. The fall in rigid fraction from 0.503 to 0.427 then represents a maximum change in polarisation/unit volume as 475 $\mu cm^{-2} K^{-1}$, assuming that all the polarisation of the Form I is lost when the rigid material is transformed to mobile material. Clearly this is an overestimate, as the mobile material clearly retains some orientation, and the molecular motions are probably limited to hindered rotation around the chain axis. The time (frequency) dependence of the pyroelectric response is also of some significance here. Pyroelectric coefficients are measured in experiments with timescales of the order of seconds. Here we are measuring crystallinities in experiments with timescales of the order of hours. This large difference must make a significant contribution to this overestimate. However, it can safely be concluded that a significant contribution to the pyroelectric coefficient can arise from the fall in crystallinity with temperature. The maximum values of the pyroelectric coefficient for PVDF are in the range 30–45 $\mu Cm^{-1} K^{-1}$.

The lower draw ratio sample shows a lower value of 0.456 for the rigid fraction, and this falls somewhat less with increasing temperature to a value of 0.423 at 60°C and to 0.405 at 80°C. These results are consistent with the distinctly lower pyroelectric coefficient of such samples.

CONCLUSIONS

(1) A satisfactory procedure has been devised for modelling the rigid lattice n.m.r. line shape in oriented PVDF in terms of a Pake doublet of superimposed Gaussian shaped lines. This procedure has been used as the basis for decomposition of the composite line into a rigid lattice doublet and a mobile component. Consistent results were obtained for the rigid mass fraction from different spectra at the same temperature. Moreover the orientation averages $\langle P_2(\cos\Delta)\rangle$ and $\langle P_4(\cos\Delta)\rangle$ deduced for this rigid component agreed extremely well with values obtained from X-ray diffraction for the orientation of the crystalline regions.

(2) The rigid mass fraction f_R was shown to decrease appreciably in the two samples examined, over the temperature range 20–80°C. Calculations show that this can give a substantial contribution to the pyroelectric coefficient. It also appears that there are differences between low draw ratio and high draw ratio samples which are in the same direction as the changes in pyroelectric response.

REFERENCES

1 Kawai, H. *Jap. J. Appl. Phys.* 1969, **8**, 975
2 Hayakawa, R. and Wada, Y. *Adv. Polym. Sci.* 1973, **11**, 1
3 Broadhurst, M. G. (Coordinator), Proceedings of Piezoelectric and Pyroelectric Symposium and Workshop, NBSIR 75-760 (US GPO Washington DC, 1975)
4 Broadhurst, M. G., Davis, G. T., McKinney, J. E. and Collins, R. E. *J. Appl. Phys.* 1978, **49**, 4992
5 Tashiro, K., Kobayashi, M., Tadokoro, H. and Fukada, E. *Macromolecules* 1980, **13**, 691
6 Kobayashi, M., Tashiro, K. and Tadokoro, H. *Macromolecules* 1975, **8**, 158
7 Bachmann, M. A., Gordon, W. L., Koenig, J. L. and Lando, J. B. *J. Appl. Phys.* 1979, **50**, 6106
8 Nix, E. L., Holt, L., McGrath, J. C. and Ward, I. M. *Ferroelectrics* 1981, **32**, 103
9 Olf, H. G. and Peterlin, A. *J. Appl. Phys.* 1964, **35**, 3108
10 McBrierty, V. J. and Ward, I. M. *J. Phys.* (D: Appl. Phys.) 1968, **1**, 1529
11 Kashiwagi, M. and Ward, I. M. *Polymer* 1972, **13**, 145
12 Smith, J. B., Manuel, A. J. and Ward, I. M. *Polymer* 1975, **16**, 57
13 Gibson, A. G. and Ward, I. M. *J. Mater. Sci.* 1980, **15**, 979
14 Richardson, A., Hope, P. S. and Ward, I. M. *J. Polym. Sci., Polym. Phys. Edn.* 1983, **21**, 2525
15 Andrew, E. R. *Phys. Rev.* 1953, **91**, 425
16 Davies, G. R. and Singh, H. *Polymer* 1979, **20**, 772
17 Van Vleck, J. H. *Phys. Rev.* 1948, **74**, 1168
18 Hasegawa, R., Takahashi, Y., Chatani, Y. and Tadokoro, H. *Polym. J.* 1972, **3**, 5, 660
19 Douglas, D. C., McBrierty, V. J. and Wang, T. T. *J. Chem. Phys.* 1982, **77**, 5826
20 Pranadi, H. and Manuel, A. J. *Polymer* 1980, **21**, 303
21 Bevington, P. R. 'Data Reduction and Error Analysis for the Physical Sciences', McGraw-Hill, 1969
22 Folkes, M. J. and Ward, I. M. *J. Mater. Sci.* 1971, **6**, 582